Retraction Notice

The Editor-in-Chief and the publisher have retracted this article, which was submitted as part of a guest-edited special section. An investigation uncovered evidence of systematic manipulation of the publication process, including compromised peer review. The Editor and publisher no longer have confidence in the results and conclusions of the article.

The authors agree with this decision.

Target recognition approach using image local features in rehabilitation robots

Milos Antonijevic[a,*] **Dijana Jovanovic**[b] **Sasa Lazarevic**[c] **Djordje Mladenovic**[b] **Milos Bukumira**[a] **and Nebojsa Bacanin**[a,*]

[a]Singidunum University, Belgrade, Serbia
[b]College of Academic Studies "Dositej," Belgrade, Serbia
[c]University of Belgrade, Faculty of Organizational Sciences, Belgrade, Serbia

Abstract. From the computer science literature, it can be seen that many different technologies are used in target recognition, which is one of the most significant areas in the artificial intelligence field. Target recognition is applied in a variety of disciplines, including healthcare, robot vision, vehicular traffic, and virtual reality. Target recognition techniques involve a robotic vision system that must perform with high accuracy and efficiency in real time; additionally, it must have the capacity to handle difficult identification contexts. In one existing target recognition system, the Harris algorithm is used; it provides a higher accuracy compared to more traditional algorithms. In order to improve its achieved accuracy, we focus on the target detection algorithm of a rehabilitation robot that is based on the local features of images. Considering the feature points of the images and target identification technology, a rehabilitation robotic recognition method is developed in this work. Initially, it collects the images, and then, adaptive weighted symplectic geometry decomposition is used for pre-processing. This method helps to reduce the noise in the images. Next, the features are extracted, and the vectors of the features are separated and identified. Afterward, one-to-many rehabilitation modes and actual system monitors are implemented to precisely select the target condition based on the functional criteria of the rehabilitation robot recognition method. Finally, an invertible color-to-grayscale conversion method using clustering and reversible watermarking is applied. It converts images into grayscale. The Gaussian distribution is consistently utilized to define the position and the quantity of the extracted feature points. Related images are retrieved as well. According to experimental findings, the proposed method improves the accuracy and the recall rate compared with the Harris algorithm. © *2022 SPIE and IS&T* [DOI: 10.1117/1.JEI.31.6.061810]

Keywords: target recognition; robots; rehabilitation robots; adaptive weighted symplectic geometry decomposition; reversible watermarking; accuracy.

Paper 220159SS received Mar. 7, 2022; accepted for publication May 6, 2022; published online Jun. 24, 2022.

Retracted

1 Introduction

The intelligence of robotic systems has become increasingly useful to human beings. Sensing qualities relatively similar to those of a human being are required for machine intelligence, which is used to investigate and analyze data; identify and enhance our awareness of various and complicated contexts; and learn about, better perceive, and increase the amount of data. Cloud servers now collect over 500 million photographs per day due to the widespread use of image capture technologies such as computers and cameras, as well as the rapid growth of virtual reality technology.

The picture feature point technique is employed in this paper to help rehabilitative robots to recognize and track targets.[1] An appropriate treatment aid system can be developed through the study of robotic systems and the investigation of the related vision technology. These systems decrease the cost and complexity of the tasks that healthcare personnel must perform because these robotic systems have enhanced processing abilities. A support program consisting of different stages guarantees that patients receive adequate and acceptable support, which includes

*Address all correspondence to Milos Antonijevic, mantonijevic@singidunum.ac.rs; Nebojsa Bacanin, nbacanin@singidunum.ac.rs

1017-9909/2022/$28.00 © 2022 SPIE and IS&T

promoting the recovery process, but also, to some extent, allows these patients to heal on their own. This program can also help to clarify the relevant concepts and to summarize the computer vision programming expertise necessary for the problem-solving procedure.

Early research on differentiable color-to-grayscale conversions has relied either on sub-band embedding (SE) or vector quantization (VQ) techniques.[2] Ordinary users can only obtain grayscale pictures due to differentiable color-image-to-grayscale-image conversions; however, authorized users can obtain high-quality visualization image features with a private key. Sub-band transform algorithms are used in SE-based methods to substitute high-frequency sub-bands with down-sampled chrominance planes. Both the grayscale image and the rebuilt color information are typically confused, resulting in a loss of high-frequency data during the upgrade process.

Traditionally, noise-reducing techniques have been divided into three categories[3]: (1) A filter removes the noisy frequencies. This noise-reducing approach is non-adaptive and requires establishing variables such as the central frequency. Furthermore, the results are not optimal for non-stationary inputs. (2) The wavelet transform (WT) splits the faulty signals into numerous individual elements and eliminates the random noise described by these faulty signals. (3) Methods like singular spectrum analysis and symplectic geometry mode decomposition (SGMD) extract eigenvalues and eigenvectors through matrix deconstruction, and then the eigenvectors associated with low eigenvalues, which are considered noise, can be eliminated.

The WT may mine the local data intensively and then retrieve those weaker faulty characteristics concealed inside a local area, just like a traditional noise reduction approach.[4–6] As a result, the WT is commonly employed in the detection of rotational equipment faults. It is indeed used for noise removal based on practical implementation effects. On the other hand, the WT has the following fundamental catastrophic flaws: (1) As the WT is a type of Fourier transformation with a variable window size, it suffers from modes in post-processing. (2) Whenever the WT dissolves the signals, it must choose a wavelet structure based on prior information. From the decomposition of the same signal, different wavelet transform sources can provide different outputs; hence, the WT is not adaptable. (3) The noise-reducing effectiveness of the WT is not perfect whenever the noise levels are too low.

An image classification technique that involves leveraging feature information gathered from input images to update the parameters and to emulate the human mind to identify the goal is demonstrated in this paper. As a result, the effectiveness of the image recognition is strongly affected by the quality of the derived features. Image categorization relies on image enhancement and selection techniques. To address the issues of slow learning speeds and reduced knowledge usage that are common in image classification networks, feature extraction is used to reduce the image dimensions and clarify the image data, allowing for the extraction of meaningful features that represent the essential nature of the target object, therefore optimizing the network's recognition performance.[7]

Beginning with the essential needs of a rehabilitation robotic platform, with rehabilitation as the objective, the main contributions of the proposed system are as follows:

1. The realization of a targeted recognition system that is relevant to the intellectual cognition, concentration, and vision areas of the field of artificial intelligence.
2. The estimation of the gray changes of complete images and the enhancement of the effectiveness and precision of the angular velocity computation used to extract the angles.
3. The use of an invertible color-to-grayscale conversion method using clustering and reversible watermarking.

The rest of this paper is organized as follows. Section 2 presents previous studies related to this research in detail. Section 3 describes the rehabilitation robots, adaptive weighted symplectic geometry decomposition (AWSGD), and reversible watermarking. Section 4 describes the experimental results, and Sec. 5 concludes this research.

2 Related Works

In some previous studies, the methods for estimating output values did not show promising outcomes, resulting in a huge difference between the experimental results and the actual robot

Retracted

interaction values.[8] In other research found in the literature, to manage prosthetic and exoskeleton robotics, researchers developed an electromyography (EMG)-based control program that utilizes EMG signals from various muscles. Pattern-matching methods are used to detect various body movements, and the categorized signals are then used as input signals to allow the control program to operate the supplementary robot components.[9]

Another study described a rehabilitation learning robot that assists in the recovery of human lower extremity function; it can participate in rehabilitation therapy that allows clients to recover their ability to walk. Smart rehabilitation electrical components can be used to assist older adults with inadequate lower extremity motor activity, as well as people with lower extremity dyskinesia induced by accidents or disasters.[10] A robot is made up of mechanical components, a process control system, and a security system, as well as a variety of sensors.[11] Such sensors, as well as the human-machine interface that operates them, could be updated on a real-time basis. Other authors have developed a human strategy that includes an attempt to accomplish real-time automated forward, upward, backward, twist, and anti-fall movements, as well as other features.[12]

Target identification and placement mechanisms, as well as a control scheme, have been widely used, for example, for robots performing compression tasks and the automated movement of trolleys.[13] To achieve robotic physical control, object searching, and orientation capabilities, a regulating system based on the humanoid robot NAO was created, and a discrete matching monocular range approach was presented. The capacity of NAO to move trolleys of various weights using visual location methods was evaluated.[14] In another study, a robot was programmed to assist stroke patients who are immobilized; the robot was programmed to assist in the flexibility rehabilitation process, such as by twisting the ankle joints and measuring the force of the ankle joints to identify the extent of the recovery of the patients.[15]

Other authors have developed an efficient reversal color-to-gray modeling approach that provided a decent performance by properly disseminating color features on only one wavelet sub-band to retain chrominance and positional accuracy. Images were divided into an indexing picture and a color scheme in the VQ-based approaches. While performing the color quantization process, the authors suggested a type of color ordering method.[16–20] A fuzzy c-means method was used for the color quantization step in the majority of cases.

The most traditional noise removal technique that uses matrices deconstruction, singular value decomposition (SVD), is employed in a variety of domains.[21,22] By deconstructing the created vector and eliminating the eigenvectors related to smaller eigenvalues, SVD decreases the amount of noise. SVD has an excellent noise-reducing impact on faulty messages with low background noise. When there is a greater amount of background noise, however, the SVD breakdown is partial, and the elements still have a significant amount of noise. To ameliorate this problem, the Lagrangian multipliers variable was introduced to minimize the noise of the decomposed component; this considerably improved the noise reduction effect.[23,24]

Non-stationary data can be processed using empirical mode decomposition (EMD).[25,26] This can deconstruct a signal into a number of useful intrinsic mode functions. On the other hand, the EMD has a number of flaws, including mode aliasing, underenveloping, overenveloping, and the lack of a formal theoretical background in terms of mathematical equation. The ensemble empirical mode decomposition (EEMD) has been developed to increase EMD's noise robustness.[27] The basic idea behind the EEMD approach is to introduce Gaussian white noise into the signal to neutralize the noise. The Gaussian white noise added by EEMD is randomized and autonomous, and the original noise will be neutralized and erased by the general average.

An eigenvalue issue involving undiscovered matrices is solved by finding the matrices analytically using the symplectic geometry similarity transformation (SGST). Then, the elements are recreated to keep the key features of the original time-series data. The symplectic geometry spectrum analysis, on the other hand, selects the embedded dimensions based on prior experience, which renders the deconstruction outcome unreliable. Pan proposed the SGMD technique,[28] which uses the power spectral density approach to flexibly calculate the embedded dimensions and the normalized mean square error limit to define the optimal solution.

A power spectral approach cannot adequately process noisy energy data. For instance, when it comes to interacting with early gear problems, this noise removal approach is not optimal. Early gearing faults are often followed by additional noise, and faulty data are not always stored in the energy elements. Whenever most of the problem data is stored in small power elements, it is

Rejected

erased following noise removal, resulting in a loss in the reliability of rapid gearing fault identification.[29] Gear problems have been determined to be associated with periodical impacts after exhaustive investigation. This periodical effect can be utilized to determine the amount of faulty data stored in these elements. Noise, on the other hand, might have a randomized affect. The study in question proposed the use of the kurtosis to define the level of the rapid effect, and conventional kurtosis could effectively quantify the periodical effect intensity of the component.[30–34]

3 Proposed Rehabilitation Robot Based on Target Recognition

The execution steps of the proposed rehabilitation robot system, are displayed in the architecture diagram shown in Fig. 1. First, the recognized image is scanned, and noise is removed using decomposition techniques. Then, the features are extracted and classified using deep learning techniques.

Target recognition methodologies have improved rapidly in recent years, and they are now extensively applied in the medical field, computer vision algorithms, navigation systems, satellite imagery, and other fields, providing tremendous assistance in people's working and personal lives.[35] Image recognition is a method of target identification that is used in robot vision applications. Figure 1 depicts the image recognition system. The initial images must first be collected and preprocessed before the extraction of features can begin. Next, each feature that is extracted from the vectors is passed to the models for recognition and classification.[36,37]

3.1 *Input Image and Pre-Processing*

First, the images are collected, and then pre-processing starts. To reduce the noise, AWSGD is used to removes the unwanted noise from the images. The AWSGD implementation generates multiple initial symplectic geometry components (ISGCs) using SGST; the ISGCs maintain the important features of the initial signal. The cycle kurtosis is then utilized to describe the

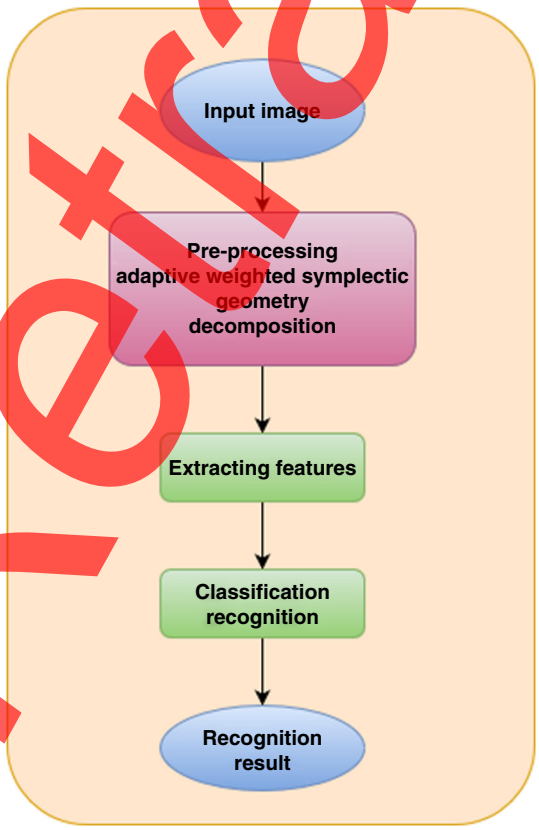

Fig. 1 Architecture of proposed system.

Retracted

periodical strength properties of the signal. The cycle kurtosis is capable of detecting repeated impacts in signals and avoids the effects of additive noise. Finally, the periodic impact intensity (PII) index is used to reject the usable elements with large amounts of faulty data, and the usable elements are weighed and reassembled by the weighting factor to produce a complete denoised symplectic geometry component.

$x = (x_1; x_2; x_N\}$ represents the initial time-series data; N denotes the time series length, and X represents the recovery matrices and the related equation is expressed as

$$X = \begin{pmatrix} x_1 & \cdots & x_{1+(k-1)\tau} \\ \vdots & \ddots & \vdots \\ x_m & \cdots & x_{m+(k-1)\tau} \end{pmatrix}, \tag{1}$$

where k represents the embedded dimensions and τ is the delayed time. Further

$$I(\tau) = \sum_{i=1}^{n-\tau} p(X_i, X_{i+\tau}) In \frac{p(X_i, X_{i+\tau})}{p(X_i)p(X_{i+\tau})}. \tag{2}$$

where $p(X_i, X_{i+\tau})$ is the combination of the probabilities of X_i and $(X_{i+\tau})$ and $p(x_i)$ in the trajectories vector represents the possibilities of x_i.

Even among the initialized symplectic geometry elements, there are many noisy elements as well as several helpful elements. The SVD eigenvalues are displayed in increasing order from the smallest to the largest. The eigenvectors related to small eigenvalues are considered noisy elements. As a result, eigenvectors with large eigenvalues are chosen for additional study. The top 10 elements are selected as research objectives after numerous sets of tests are compared. The element attributes are judged according to the amount of constituent energy in the SVD and SGMD procedures. The beneficial elements have excellent properties, whereas the noisy elements have reduced the energy content. The beneficial elements have a high kinetic energy, whereas the noisy elements have a lower power content. The PII is developed to measure the position information of a module. This not only eliminates the risk of noise removal related to the energy magnitude but also eliminates the effect of the actual impact and the equations are expressed as

$$\mathrm{CK}_{\mathrm{mean}} = \frac{\sum_{i=1}^{k} \mathrm{CK}_i}{k}, \tag{3}$$

$$\mathrm{PII}_1 = \frac{\mathrm{CK}_i}{\mathrm{CK}_{\mathrm{mean}}}. \tag{4}$$

The value PII_i can now be used to assess the magnitude of periodical influence on the components. The bigger the PIIi value is, the greater the periodical effect of the components; this also means that the element has more faulty information. It is necessary to choose beneficial components that hold more faulty information to eliminate the volume of noise in the earliest signals and it is given by

$$Y = \sum_{i=1}^{k} \mathrm{PII}_i \times P_i. \tag{5}$$

3.2 *Extracting and Selecting the Features*

Visual classification is a technique that involves leveraging feature data gathered from the input images to train the system and emulate human brain activity in order to identify the goal. As a result, the effectiveness of the image recognition is strongly affected by the quality of local image features. The core technologies in image categorization are image enhancement and selection techniques. In order to address the issues of a slow learning density and a reduced data utilization rate in image classification networks, feature extraction is used to reduce the image dimensions and summarize the image data, allowing the extraction of meaningful features that represent the essential nature of a target object; this allows the optimization of the network recognition accuracy.

Retracted

Extracting features involves extracting the information that represents a picture from raw image data using various function modifications.[38] Popular linearization approaches include principal component analysis (PCA) and linear discrimination.[39,40] The PCA begins by orthogonally transforming a set of inputs; then, the largest variation of the set is calculated, and finally the group with the greatest variation is selected as the PCA features of the initial linear subset of features. Lastly, the PCA characteristics are ordered, and the top-ranked selected features are chosen as additional features, with the goal of lowering the complexity of the initial image.

3.3 *Rehabilitation Robot Module's Functional Requirements*

3.3.1 *"One-to-many" rehabilitation state and system monitoring in real time*

This device is capable of providing entirely automated support, allowing a physician to choose rehabilitation objectives and measure the rehabilitation process for several patients on a real-time basis, i.e., it is a "one-to-many" rehabilitation model.[41] To begin, healthcare professionals use the master software program to choose different rehabilitation assignments for several patients from the program's rehabilitation goal libraries; these tasks are assigned to various patients as required. The rehabilitation framework and auxiliary rehabilitation surroundings are identical for each client, and the supplementary rehabilitation procedures can be automated and self-serviced; as a result the physician can supervise the rehabilitation process of every patient using the central control gateway application and cameras.[42] According to the Wechsler Adult Intelligence Scale's technique for assessing cognitive aptitude, basic elements can be used to teach cognitive processes such as memorization, concentration, and the visualization of spaces.

3.3.2 *Recognizing blocks*

To assist in cognitive training with construction blocks, the system must be capable of recognizing the main section of a construction block against complex background scenes. This involves the capacity to focus on the block within surrounding areas with different light sources, backdrop patterns, and angle shifts, as well as other factors that may interfere. An individual block must be identified. Second, the system is required to retrieve appropriate characteristics for various building types of the elements, recognize various types of structures, and perform target recognition and feature parameter collection. Third, the solution should be designed to recognize targets and matched parameters depending on the multiple kinds of activity images. This allows job visuals to be created by splicing two or more construction blocks together, and the system must be able to complete the recognition using applicable visual techniques.

3.3.3 *Allowing patients to communicate with the machine through the help button*

It is not possible to achieve interaction, within the rehabilitation training program, by individuals with intellectual disabilities if they must write computer programs and memorize complicated operational procedures.[43] Thus, the technology itself must have great human communication abilities. The relevant instructions are presented to the patient very naturally through the software window on the output device. A patient must merely push a key, even during the information transmission process, to receive assistance.

3.3.4 *Generating applicable puzzle approaches and operating the teaching robotic arm*

Throughout the supported rehabilitation program, the system should be able to distinguish between various types of blocks inside the targeted visuals and the scattered construction blocks on the working surface. The system must use the positions of the blocks according to the real work framework as well. Then, relevant data, including phase differences, are used to build the problem approach. A targeted visual, for instance, is made up of two pieces, which are labeled as

Retracted

block 1 and block 2. For the sake of completing the game, the system must be able to transfer block 1 to block 2 without collision, and it must be capable of modifying the phase of block 1. After this, the system should independently manage the mechanical arm so that it can substitute for the clinical professionals, as well as follow the appropriate approach for completing the tasks assigned to the patient.[28,44]

3.4 *Invertible Color-to-Grayscale Conversion Method Using Clustering and Reversible Watermarking (ICGRW)*

The development of the color palettes, the embedding of the color palettes, the creation of the grayscale images, and the reconstruction of the color images are the four fundamental parts of invertible conversions between color and grayscale images. In a previous study,[2] the authors proposed a strategy that is equivalent to the one described here. Rather than using the convex hull creation approach to reduce the square errors, a k-means clustering-based approach is used to build the color palettes. Additionally, by utilizing reversible watermarking, the embedding procedure based on least significant bit (LSB) replacement[2] is enhanced; this procedure not only accurately extracts the color palette but also recovers the image representation with no losses. A proposed methodology for creating the color palette is depicted in Fig. 2; the goal is to design a color palette that is excellent at expressing the original color picture CI with little distortion and at producing a color-embedded grayscale image GIC that is equivalent to the luminance planes of the color image.

3.4.1 *Color palette generation*

As the CIELAB color structure is predicated on physiological measurements, the color palette is created in this color space. A given amount of quantitative change in the CIELAB color space is comparable to the changes seen by the visual system. A conversion from the red green blue (RGB) space to the CIELAB space is necessary whenever image data are described in the RGB format. Following this conversion, the pixels are computed separately (L, A, B), where L denotes the luminance and A and B denote the corresponding chrominance elements. Given that eight-bit grayscales image data have only 256 gray values, the color palette should be 256 colors. Furthermore, a one-to-one mapping of the image pixels of the grayscale image to the color palette is preferable so that distinctive color data can be established to recreate the color image. As a result, the goal is to discover 256 alternative colors to represent all of the colors in the natural color picture, which requires quantification of the luminance planes, A planes and B planes into a 256×3 vector. As illustrated in Eq. (6), one popular method is to partition the CIELAB area into 256 periods, according to the brightness directions and the equation is expressed as

$$L_{(k)} = (L_{k,\mathrm{UB}} + L_{k,\mathrm{LB}})/2. \tag{6}$$

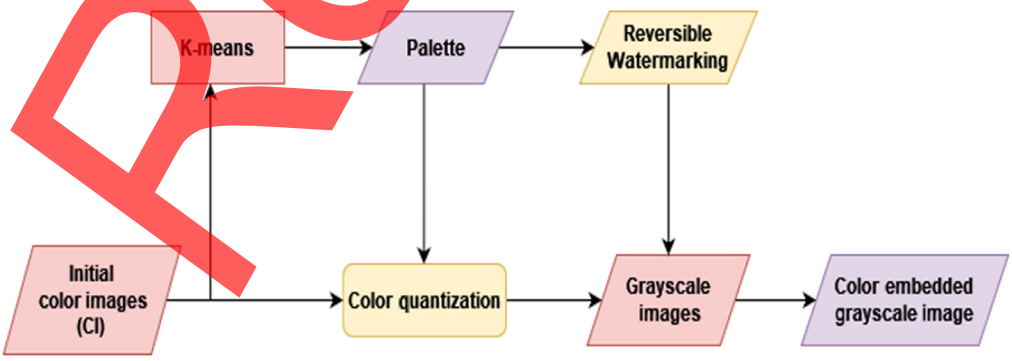

Fig. 2 Process of coding.

Retracted

The minimum and maximum luminance ratios in certain intervals are represented by $L_{k,\mathrm{UB}} + L_{k,\mathrm{LB}}$, respectively. The variance in visible colors inside the intermediate periods is greater than the variance in the up or down periods.[2]

3.4.2 *Creations of grayscale images*

When all of the colors in picture CI been quantized to the frequencies of the generalized color scheme, the image data may be formed using the address of the color palette after the color scheme has been built. If one pixels is represented by $\mathrm{CI}_{i,j}$ and the luminance element is represented by $L_{i,j}$, the quantization luminance element's layer is calculated according to the equation which is expressed as

$$k \in L_{k,\mathrm{UB}} > L_{i,j} > L_{k,\mathrm{LB}} \quad \text{and} \quad 53 \geq k \geq 0. \tag{7}$$

The chrominance of $C_{i,j}$ is normalized to a cluster of a current frame after the luminance level to which $C_{i,j}$ is related is determined by the equations

$$\lambda - \arg\min_{\lambda=1,2,\ldots,N_k} \| C_{i,j} f(\vec{p} f_0(k,\lambda) \|^2, \tag{8}$$

$$\mathrm{CI}_{\mathrm{quan}(i,j)=} P_{f_{0(k,\lambda)}}, \tag{9}$$

$$\mathrm{GI}_c(i,j) = f_0(k,\lambda). \tag{10}$$

This reference image now functions as a 256-level grayscale image that matches the input image CI.

3.4.3 *Color palette reversible embedding*

The color palette must be incorporated into to the grayscale image after the creation of the color palette and the grayscale images for gray-to-color conversion. The LSB replacement is commonly utilized in the literature to encode color schemes.[2] The main idea behind the LSB replacement is to replace the least relevant byte of the grayscale with color palette's bit stream. The absence of the restored data, on the other hand, will affect the grayscale image to a certain extent, leading to further distortion of the restored composite image. As a result, an excellent way to solve this issue is to utilize a technology that can retrieve the image representation with no loss while rebuilding the color image and recover the color palette from the color-embedded gray image.

Because an irreversible embedded watermark may fulfill the criterion of retrieving the main image in a lossless manner,[2] the reversible data hiding method is used[2] to embed the color palette in the proposed study. A feasible and simple technique for achieving the requirement of validating the information consistency in transport is to hash the grayscale and insert the hash code.

4 Performed Experiments, Discussion, and Analysis

4.1 *Simulation Environment*

The technique in this work was implemented using VS2013 + OpenCV2.4.9 and executed on an Intel Core (TM)i3-2350M CPU running at 2.30 GHz with 6 GB of RAM.

4.2 *Data Collection*

The proposed method was validated against an affine covariant regions dataset, and Harris algorithm along with Harris in combination with scale-invariant feature transform (SIFT) as comparative techniques. The data input for each learning experiment consists of 600 K samples

Retracted

Table 1 Data statistics of feature matching using algorithms.

Algorithms	Total matching point pairs	Point pairs correctly matched	Point pairs mismatched	Point pair missing match	*F*1 (%)	Accuracy (%)	Recall rate (%)
Harris	493	397	216	208	67.70	62.30	63.10
SIFT + Harris	484	372	339	214	56.60	52.30	56.10
Proposed algorithm	495	403	210	201	71.52	68.35	67.78

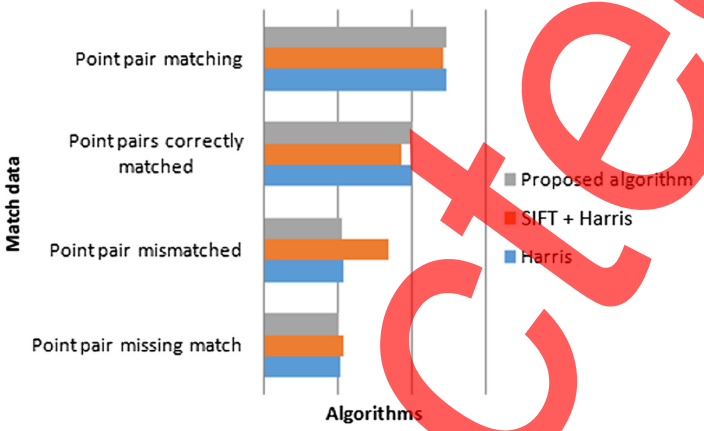

Fig. 3 Comparison of feature matching.

that are created from the predefined training sample of the utilized dataset. For testing purposes, 50 K positive samples and 50 K negative samples are chosen from the test set of the employed dataset. The FPR95 (Error at rate of 95%)166] is used as the test index. A lower FPR95 value indicates a better algorithm performance.[45]

4.3 *Comparison of Feature Matching Experiment*

Data were statistically analyzed on matching point pairings after features matching were conducted on features extraction images. Table 1 summarizes experimental findings in terms of *F*1-score, accuracy, and recall metrics, and the Fig. 3 depicts the feature matching data diagram for the compared methods.

4.4 *Time Taken for Mismatched Point Pairs*

The utilized ICGRW method outperforms other state-of-the-art techniques, such as recursive random sample consensus (R-RANSAC), in terms of needed time to eliminate mismatched point pairs. It is computationally efficient, and it decreases computation time to 1392 ms on average compared with R-RANSAC, while maintaining feature-based accuracy. Figure 4 shows the time taken to eliminate the mismatched point pairs by comparative analysis.

4.5 *Accuracy*

Another experiment conducted for this study refers to the accuracy. Due to the neighbor distance ratio method being one of the most widely adopted techniques in local feature descriptor matching, this technique is also utilized in this experiment. Figure 5 depicts the accuracy verification of the nearest neighbor feature matching method. The accuracy of the nearest neighbor feature matching method is 39.75% for 50% of image pairs.

Retracted

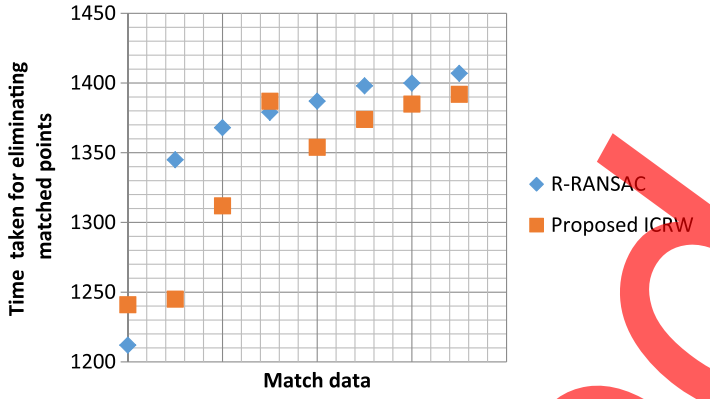

Fig. 4 Comparison of time taken for eliminating the mismatched points.

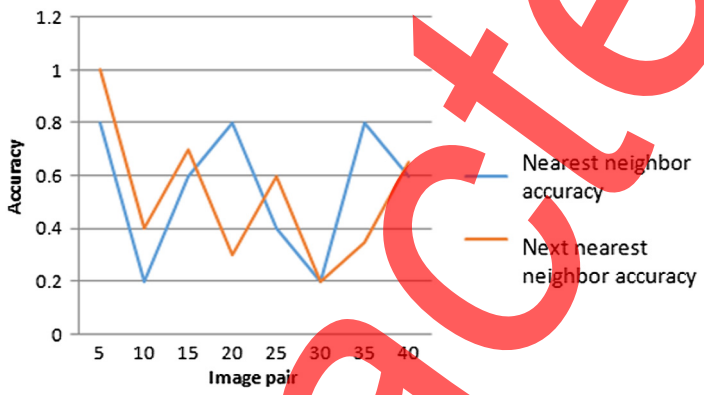

Fig. 5 Verification of nearest neighbor accuracy.

4.6 *Target Recognition Test for Rehabilitation Robot*

The evaluation of the target recognition ability of the rehabilitation robot and its tracking abilities in a real-world setting is performed. In PASCAL VOC[1] the rehabilitation robot can distinguish 20 different target items. Therefore, this work presents a learned target recognition model with improved accuracy. A person was chosen as a target for testing in this experiment. The following are the outcomes of the test: the angular displacements between the targets as well as the rehabilitation robots vary under the conditions of a constant monitoring range of 150 cm. The very first set of tests have been completed. Angular displacement of rehabilitation robots is shown in Fig. 6.

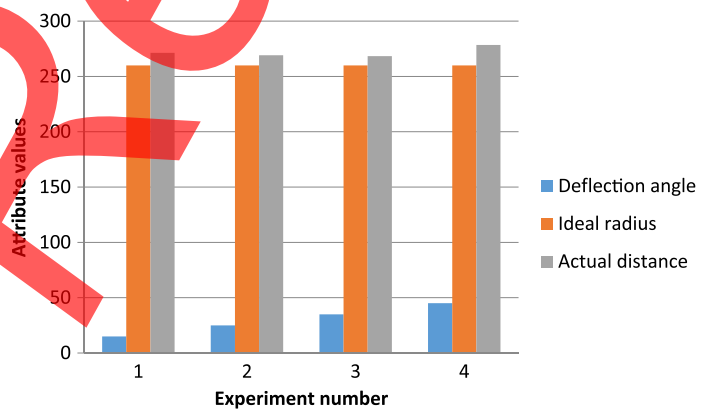

Fig. 6 Comparing angles of rehabilitation robots.

Retracted

5 Conclusion

The use of machine vision in the field of medicine is discussed in this study. Rehabilitation robots and target identification and placement offer a comprehensive vision solution. This visionary solution could be used with a laser to find a round work-piece in industrial applications with millimeter-level positional precision. Similar to industrial uses, a vision system also offers great adaptability to various situations. This topic is also a point of reference for comparable vision-based situations. This vision solution is ideal for higher-precision positioning needs. Current systems are unable to meet acceptable standards, which necessitates enhancing the calibration efficiency of the visual system or enhancing the visual positioning algorithms. This study focused on a rehabilitation robot's target identification system, which was adapted to the local features of images in order to increase its accuracy.

In this paper, the rehabilitation robotic recognition methodology is based on the image features and target identification technologies. This method gathers the images first, and then uses adaptive weighted symplectic geometry decomposition for pre-processing. This technique aids in the reduction of visual noise. The characteristics are then retrieved, and their vectors are separated and identified. Next, considering the functional conditions of the rehabilitation robotic detection and recognition, one-to-many rehabilitation methods and real system monitoring are applied to precisely choose the target state. The study focused on the necessary algorithms and technology platforms, which include computer vision and a graphical interface. A Fourier description operation is used to identify targets once the system has pre-processed the input image. The study next presents a modulus displacement method for extracting the targeted image-related variables without even being influenced by the initial state of the image edge. Therefore, the proposed method improves the accuracy, recall, and time taken to eliminate mismatched point pairs.

Retracted

References

1. X. Li and T. Wu, "Target recognition method of rehabilitation robot based on image local features," *IEEE Access* **8**, 160607–160615 (2020).
2. Q. Liang et al., "Invertible color-to-grayscale conversion by using clustering and reversible watermarking," in *IEEE Int. Conf. Multimedia and Expo (ICME)*, IEEE, pp. 1–6 (2021).
3. J. Cheng et al., "A noise reduction method based on adaptive weighted symplectic geometry decomposition and its application in early gear fault diagnosis," *Mech. Syst. Signal Process.* **149**, 107351 (2021).
4. L. Xin et al., "A robust white-light interference signal leakage sampling correction method based on wavelet transform," *Opt. Lasers Eng.* **133**, 106156 (2020).
5. N. Kumar and R. Kumar, "Wavelet transform-based multipitch estimation in polyphonic music," *Heliyon* **6**(1), e03243 (2020).
6. M. El-Hendawi and Z. Wang, "An ensemble method of full wavelet packet transform and neural network for short term electrical load forecasting," *Electr. Power Syst. Res.* **182**, 106265 (2020).
7. S. Wan et al., "Deep learning models for real-time human activity recognition with smartphones," *Mob. Networks Appl.* **25**(2), 743–755 (2020).
8. M. Abd El Aziz et al., "Prediction of biochar yield using adaptive neuro-fuzzy inference system with particle swarm optimization," in *IEEE PES PowerAfrica*, IEEE, pp. 115–120 (2017).
9. X. Zhang et al., "sEMG-based shoulder-elbow composite motion pattern recognition and control methods for upper limb rehabilitation robot," *Assembly Autom.* **39**(3), 394–400 (2019).
10. M. Abdel-Basset et al., "Evaluation framework for smart disaster response systems in uncertainty environment," *Mech. Syst. Signal Process.* **145**, 106941 (2020).
11. W. Elsayed et al., "Self-maintenance model for wireless sensor networks," *Comput. Electr. Eng.* **70**, 799–812 (2018).
12. Y. Qiao et al., "A rehabilitation robot and its industrial design for human lower limb training," *Trans. Beijing Inst. Technol.* **37**(7), 698–703 (2017).

13. L. Wu et al., "A mobile positioning method based on deep learning techniques," *Electronics* **8**(1), 59 (2019).
14. L. Zhang et al., "Target recognition of indoor trolley for humanoid robot based on piecewise fitting method," *Int. J. Adapt. Control Signal Process.* **33**(8), 1319–1327 (2019).
15. J.-H. Jung and G.-S. Kim, "Development of an ankle rehabilitation robot for ankle-bending rehabilitation exercise," *J. Inst. Control Rob. Syst.* **22**(1), 31–39 (2016).
16. M. Chaumont and W. Puech, "Protecting the color information by hiding it," *Recent Adv. Signal Process.* **22**, 101–122 (2009).
17. M. Chaumont and W. Puech, "A fast and efficient method to protect color images," *Proc. SPIE* **6508**, 65081T (2007).
18. M. Chaumont et al., "Securing color information of an image by concealing the color palette," *J. Syst. Software* **86**(3), 809–825 (2013).
19. M. Chaumont and W. Puech, "A grey-level image embedding its color palette," in *IEEE Int. Conf. Image Process.*, IEEE, Vol. 1, pp. I-389–I-392 (2007).
20. M. Shanmugam and R. Asokan, "A machine-vision-based real-time sensor system to control weeds in agricultural fields," *Sens. Lett.* **13**(6), 489–495 (2015).
21. H. Li et al., "Fast multidimensional NMR inversion based on randomized singular value decomposition," *J. Pet. Sci. Eng.* **190**, 107044 (2020).
22. M. Zhao and X. Jia, "A novel strategy for signal denoising using reweighted SVD and its applications to weak fault feature enhancement of rotating machinery," *Mech. Syst. Signal Process.* **94**, 129–147 (2017).
23. M. Zeng et al., "μ-SVD based denoising method and its application to gear fault diagnosis," *J. Mech. Eng.* **51**(3), 95–103 (2015).
24. S. Maheswaran et al., "Embedded system based an automatic coconut dehusker with identification of decay in copra for export packaging," *Int. J. Print. Packaging Allied Sci.* **4**(1), 592–601 (2016).
25. C. Wang et al., "Wind power forecasting based on singular spectrum analysis and a new hybrid Laguerre neural network," *Appl. Energy* **259**, 114139 (2020).
26. X. Mi and S. Zhao, "Wind speed prediction based on singular spectrum analysis and neural network structural learning," *Energy Convers. Manag.* **216**, 112956 (2020).
27. H.-B. Xie et al., "Symplectic geometry spectrum analysis of nonlinear time series," *Proc. Math. Phys. Eng. Sci.* **470**(2170), 20140409 (2014).
28. S. Pan et al., "Learning graph embedding with adversarial training methods," *IEEE Trans. Cybern.* **50**(6), 2475–2487 (2019).
29. A. Chuhutin et al., "Diffusion kurtosis imaging maps neural damage in the EAE model of multiple sclerosis," *NeuroImage* **208**, 116406 (2020).
30. D. Wang et al., "The sum of weighted normalized square envelope: a unified framework for kurtosis, negative entropy, Gini index and smoothness index for machine health monitoring," *Mech. Syst. Signal Process.* **140**, 106725 (2020).
31. X. Wang et al., "Diffusion kurtosis imaging combined with molecular markers as a comprehensive approach to predict overall survival in patients with gliomas," *Eur. J. Radiol.* **128**, 108985 (2020).
32. S. Shukla et al., "An efficient heart sound segmentation approach using kurtosis and zero frequency filter features," *Biomed. Signal Process. Control* **57**, 101762 (2020).
33. J. Antoni, "The infogram: entropic evidence of the signature of repetitive transients," *Mech. Syst. Signal Process.* **74**, 73–94 (2016).
34. S. Maheswaran et al., "Unmanned ground vehicle for surveillance," in *11th Int. Conf. Comput., Commun. and Networking Technol. (ICCCNT)*, IEEE, pp. 1–5 (2020).
35. S. Wan and S. Goudos, "Faster R-CNN for multi-class fruit detection using a robotic vision system," *Comput. Networks* **168**, 107036 (2020).
36. P. Prokazova et al., "Robot-assisted therapy using the MOTOmed letto 2 for the integrated early rehabilitation of stroke patients admitted to the intensive care unit," *Hum. Physiol.* **42**(8), 885–890 (2016).
37. I. Yildiz, "A low-cost and lightweight alternative to rehabilitation robots: omnidirectional interactive mobile robot for arm rehabilitation," *Arab. J. Sci. Eng.* **43**(3), 1053–1059 (2018).

Rejected

38. E. L. Lydia et al., "Application of discrete transforms with selective coefficients for blind image watermarking," *Trans. Emerg. Telecommun. Technol.* **32**(2), e3771 (2021).
39. B. Fan et al., "A performance evaluation of local features for image-based 3D reconstruction," *IEEE Trans. Image Process.* **28**(10), 4774–4789 (2019).
40. U. Raju et al., "Content-based image retrieval using local texture features in distributed environment,"*Int. J. Wavelets Multiresolut. Inf. Process.* **18**(1), 1941001 (2020).
41. B. Zhao et al., "Deep pyramid generative adversarial network with local and nonlocal similarity features for natural motion image deblurring," *IEEE Access* **7**, 185893–185907 (2019).
42. S. Zhou et al., "Multi-camera transfer GAN for person re-identification," *J. Vis. Commun. Image Represent.* **59**, 393–400 (2019).
43. J. Jiang et al., "Recent patents on end traction upper limb rehabilitation robot," *Recent Pat. Mech. Eng.* **10**(2), 102–110 (2017).
44. R. Wang et al., "A formal model-based design method for robotic systems," *IEEE Syst. J.* **13**(1), 1096–1107 (2018).
45. Y. Zhao and C. Yang, "Information fusion robust guaranteed cost Kalman estimators with uncertain noise variances and missing measurements," *Int. J. Syst. Sci.* **50**(15), 2853–2869 (2019).

Biographies of the authors are not available.

Retracted